Available online at www.sciencedirect.com

ScienceDirect

journal homepage: www.elsevier.com/locate/he

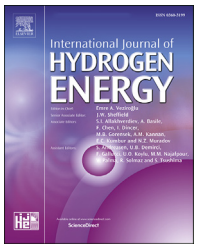

On the reduction of $NiFe/Al_2O_3$ oxygen carrier in high-pressure chemical looping applications

Orlando Palone [a,b], *Rouzbeh Ramezani* [a], *Claudia Navarro* [c], *Luca Di Felice* [a], *Domenico Borello* [d], *Gemma Grasa* [c], *Fausto Gallucci* [a,*]

[a] *Sustainable Process Engineering, Department of Chemical Engineering and Chemistry, Eindhoven University of Technology, De Rondom 70, 5612 AP, Eindhoven, the Netherlands*

[b] *Department of Astronautical, Electrical and Energy Engineering, Sapienza University of Rome, Via Eudossiana 18, 00184, Rome, Italy*

[c] *Instituto de Carboquímica - ICB-CSIC, Miguel Luesma Castán 4, 50018, Zaragoza, Spain*

[d] *Department of Mechanical and Aeronautical Engineering, Sapienza University of Rome, Via Eudossiana 18, 00184, Rome, Italy*

HIGHLIGHTS

- Chemical looping cycles were carried out at ambient and high-pressure conditions.
- Full reduction conversion was achieved at 900 °C after 200 s of testing for a nickel ferrite with 12% wt Ni and 8.5% wt Fe.
- Total pressure showed a negative effect on reaction kinetics.
- No significant changes in the microstructure of the material were observed.

ARTICLE INFO

Article history:
Received 9 July 2023
Received in revised form
15 September 2023
Accepted 21 September 2023
Available online 10 October 2023

Keywords:
Chemical looping
High pressure
Hydrogen reduction
Nickel–iron
Redox

ABSTRACT

Chemical looping represents a promising technology with various applications ranging from clean power production to alternative syngas production. In this work, two oxygen carriers with different Ni loadings (4.3% wt. and 12% wt.) and similar Fe loadings (9.9% wt. and 8.5% wt.) are synthesized through a co-precipitation/impregnation route and tested in two thermogravimetric analyzers. Firstly, the effect of temperature (700–900 °C) on the oxygen transport capacity and reduction conversion of both materials is assessed at ambient pressure (0.5 nl/min with 20% H_2/N_2). The influence of material loading is also studied, and it is shown that higher Ni loadings provide a significant improvement in material activity. A complete reduction conversion is achieved at 900 °C and ambient pressure. At high pressure (10–20 bar), tests are carried out in a temperature range of 700–850 °C. The effect of flow rate (2 nl/min to 6 nl/min with 50% H_2/N_2) is first assessed to prevent external mass transfer limitations. Higher total pressures have a negative effect on reduction kinetics, while higher Ni loadings demonstrate increased final reduction conversion also at high pressure, reaching about 75% conversion after 20 min. The long-term cyclability of the material is also investigated both at low (100 cycles) and high pressure (80 cycles) conditions and a conversion gain is observed throughout the cycles in both cases. No changes in the material microstructure are observed after 80 high-pressure cycles.

* *Corresponding author.*
E-mail address: f.gallucci@tue.nl (F. Gallucci).

https://doi.org/10.1016/j.ijhydene.2023.09.235

1. Introduction

Chemical looping represents a promising technology due to its numerous fields of application and its inherent CO_2 separation properties. In chemical looping combustion (CLC) a metal oxide (Me_xO_y/MeO), also known as an oxygen carrier, undergoes two subsequent reaction steps: reduction and oxidation. In the fuel reactor, the metal oxide is reduced by reacting with a fuel, either solid (solid carbon or biomass) or gaseous (methane, syngas, or other hydrocarbons), while in the air reactor, the reduced material is oxidized by reaction with air [1]. The output gases from the fuel reactor are CO_2 and H_2O, which facilitate the capture and subsequent storage of high-purity CO_2 after water condensation, while depleted air is the output of the air reactor. One of the most valuable properties of chemical looping is the intrinsic separation of CO_2 and N_2 from fuel combustion gases, allowing clean power production by integration with CO_2 storage. In this way, the cost, and the energy penalty (at least 8%–12% thermal efficiency reduction [2]) associated with the retrofitting of traditional power plants with CO_2 capture and storage units is avoided. The most widespread configuration for chemical looping cycle operation is the interconnected fluidized beds, where the oxygen carrier circulates between the fuel and the air reactor, while the high enthalpy gas stream from the air reactor is utilized for power production in a turbine group and/or steam generation. Other configurations such as moving bed and packed bed reactors have also been extensively analyzed in the literature and are more suitable for high-pressure operations. In fact, to be competitive with current power plants, chemical looping plants need to be operated at high temperatures (above 800 °C) and pressure conditions (about 20 bar). Thermodynamic analysis has indicated that by coupling pressurized chemical looping combustion with a combined cycle fed with natural gas, the thermal efficiency can reach values between 52% and 55% [3,4] when high temperatures and pressures are enforced.

A key issue for the development of the chemical looping technology is the selection of an oxygen carrier with suitable properties. The oxygen carrier must accomplish several characteristics such as sufficient oxygen transport capacity, high reactivity for reduction and oxidation reactions, minimum solids inventory in the reactors, stability over many successive redox cycles, negligible carbon deposition (that would release CO_2 in the air reactor reducing the CO_2 capture efficiency), environmentally friendly characteristics, low cost and large availability [5,6]. There are more than 900 different materials based on iron, nickel, copper, manganese, as well as other mixed oxides and low-cost materials that have been investigated as potential oxygen carrier materials for chemical looping applications [7].

Nickel-based oxygen carriers have been the most extensively analyzed in the literature [8], due to their very high reactivity, good performance working at high temperatures and low attrition rates. Iron-based oxygen carriers are another attractive option for chemical looping due to their low cost, large availability and environmental compatibility [9]. Regarding Fe-based oxygen-carriers, different oxidation states can be found when Fe_2O_3 is reduced (Fe_3O_4, FeO or Fe) and thus flexibility for different chemical looping applications is ensured, such as chemical looping combustion, reforming or H_2 production However, iron oxides suffer from agglomeration and sintering when operated at high temperatures and require support with other materials to be competitive for chemical looping applications [10]. The most common support materials are Al_2O_3 [11,12], monoclinic ZrO_2, partially stabilized tetragonal zirconia (t-PSZ), yttria-stabilized cubic zirconia (c-YSZ), titanium dioxide (TiO_2), manganese oxide, bentonite, and their mixtures [13]. Adanez et al. [14] analyzed 240 samples of Cu, Fe, Mn and Ni oxides under reduction and oxidation cycles to assess the optimal active phase content, sintering temperature and support material among Al_2O_3, sepiolite, SiO_2, TiO_2 and ZrO_2. The use of alumina-based compounds as support material has been extensively investigated in the literature, due to their benefits in terms of long-term stability of the oxygen carrier. Most of the oxygen carriers supported on Al_2O_3 compounds show very high reactivity with all fuel gases, no agglomeration problems, low attrition rates during operation in fluidized beds and avoidance of carbon deposition at CLC conditions [15]. Nevertheless, Al_2O_3 can interact with the active phase of the oxygen carrier, such as Fe_2O_3, and form spinel structures that change the particle reactivity. In chemical looping hydrogen production, the formation of $FeAl_2O_4$ (hercynite) is indicated as the reason for oxygen carrier deactivation, because it is inert to the steam iron-reaction. A third step with air oxidation or a low mass loading (few percentage) of Al_2O_3 is suggested as possible solution for the regeneration of Fe_2O_3 and Al_2O_3 from the hercynite structure [16–19]. On the contrary, Ni/Al_2O_3 and NiO/$NiAl_2O_4$ oxygen carriers have proved high reactivity in chemical looping combustion of gas fuels (CH_4, CO and H_2), as well as good chemical, mechanical and reactive stability [20]. The formation of $NiAl_2O_4$ by the interaction of free NiO with the Al_2O_3 support is however responsible for a decrease in the oxygen carrier reactivity. Dueso et al. [21] showed that irrespective of the final solid conversion in the reduction of NiO/Al_2O_3, 80% of the reacted oxygen carrier is regenerated to free NiO and the rest to less reactive $NiAl_2O_4$.

In order to limit the drawbacks associated with iron oxides as oxygen carriers, an increasing number of studies have focused on combined or mixed-metal oxides. In Ref. [22], bimetallic Fe–Ni compounds with Al_2O_3 and CeO_2 support were compared with iron and nickel oxides by Bhavsar et al. Increased stability and higher selectivity towards fuel oxidation were observed for the bimetallic compound compared to a simple supported iron oxide, similar to the observations by Kuo et al. [23]. Increased reactivity when a reactive support (CeO_2) is present was also highlighted. Evdou et al. [24], compared the performance of different ferrites incorporating Mn, Ni, Zn, Co and Cu. Cu ferrite showed the highest reactivity towards methane and good stability, Ni and Zn presented high reactivity but fast deactivation after few cycles due to sintering (Ni/Fe) or phase decomposition (Zn/Fe), while Co presented the best stability configurating as a promising active support. In Refs. [25,26], due to the catalytic effect of metallic Ni, the bimetallic Fe–Ni oxygen carrier provided improved gasification efficiency compared to Fe_2O_3/Al_2O_3. On the same line, Wei et al. [27] compared four different ferrites (Ba, Ni, Cu and Co ferrites) for chemical looping gasification of biomass in

a fixed-bed reactor. Though all four ferrites showed improved gasification performance with respect to an inert bed, Ba ferrite provided the highest syngas yield and H_2 content from biomass gasification as well as good tar cracking performance. Finally, Wang et al. [28] compared Ni, Cu and Co ferrite for chemical looping combustion of pine sawdust. All three ferrites provided high values of carbon conversion and carbon capture efficiency (around 95%), though after five cycles only Cu and Co ferrites kept stable values. On the contrary, Ni ferrite provided higher catalytic activity for tar cracking and reforming at every tested temperature.

Iron and nickel-based oxygen carriers have also been extensively studied in the literature for chemical looping reforming processes [29–31]. Compared to the traditional reforming processes, the most immediate advantages of chemical looping reforming are the absence of the air separation unit for pure oxygen production (necessary for the autothermal reforming) and the intrinsic CO_2 separation. Ortiz et al. [32] investigated the catalytic activity of two Ni-based oxygen carriers for both the steam methane reforming and the water gas shift reactions and showed that the activity increases with the reduction conversion of the oxygen carrier. Comparison with conventional catalysts indicated a lower catalytic activity of the oxygen carriers. Huang et al. [33]. Compared nickel oxides (NiO, mixed NiO and Fe_2O_3, NiFe) and iron oxides (Fe_2O_3) for chemical looping dry reforming applications. The process encompassed three steps: reduction with methane and oxidation with CO_2 and then air. Nickel ferrite proved to better dissociate CO_2 in the first oxidation step due to its spinel structure, while metallic nickel did not show any oxidizability with CO_2. Antzara et al. [34] analyzed the effect of different supports (ZrO_2, TiO_2, SiO_2, Al_2O_3) on NiO in terms of CH_4 conversion and long-term stability both as conventional catalysts and in chemical looping reforming. SiO_2 and TiO_2 supports lead to poor performances (low activity and fast deactivation) as conventional catalysts. The other supported materials (Al_2O_3 and ZrO_2) were tested for chemical looping reforming and ZrO_2 resulted to have the best stability after 20 cycles (less than 2% decrease in the activity) as well as a competitive methane conversion.

1.1. *High-pressure chemical looping*

High-pressure operation represents an important condition for industrial scale-up of chemical looping [35]: in chemical looping combustion high-pressures are mandatory to better exploit the enthalpic content of the off-gases for power generation in a combined cycle power plant rather than a Rankine cycle power plant; in chemical looping reforming, high-pressure facilitates the downstream processing of syngas to liquid fuels [36], such as methanol [37], ammonia [38], kerosene [39] etc., thus reducing the total equipment cost and the carbon footprint of the process. High pressure operation also impacts the process design of the reactors; e.g. in fluidized bed reactors high pressure leads to smaller and more frequent bubble formation, lower minimum fluidization velocities and terminal velocities (easier elutriation) [40]. Furthermore, a change in kinetics at high-pressure influences the choice of the optimal thermodynamic conditions and of reactor geometry to achieve the desired solid conversion and products composition.

Several works in the literature present data on high-pressure chemical looping cycles. In Ref. [41], a comparative analysis between chemical looping coal combustion in fixed bed and fluidized bed configurations was carried out at high pressure conditions by Zhang et al. The results indicated that up to 0.5 MPa total pressure has a beneficial impact on gasification while the opposite holds for higher values in both cases. However, the fixed bed configuration showed enhanced carbon conversion and CO_2 production, but with a higher risk of agglomeration and sintering over long-term operation. Gallucci et al. [42] tested ilmenite in a pressurized 10 kW packed bed reactor for the chemical looping combustion of syngas. The setup reached a steady state operation after about three cycles and the effect of syngas composition and total pressure (maximum 6 bar) was discussed. A model was also developed and validated for the description of the experimental results. Argyris et al. [29] investigated methane chemical looping reforming with $NiO/CaAl_2O_4$ as the oxygen carrier in a lab scale reactor under different temperatures (400–900 °C), pressures (1–5 bar) and flowrates (10–40 NL/min). Full autothermal operation was demonstrated along with >99% CH_4 conversion. Hamers et al. [43] reported experimental evidence on the reactivity of CuO/Al_2O_3 and $NiO/CaAl_2O_4$ for chemical looping combustion under high pressure conditions. The effect of pressure was shown to be detrimental for reaction kinetics while different reducing gas molar fractions provided different reduction behavior, likely due to a competitive adsorption mechanism. Garcia-Labiano [44] tested the reactivity of Cu, Fe and Ni-based oxygen carriers for chemical looping at 450–900 °C and 1–30 bar and provided an expression for the reaction kinetics at high pressure. The negative effect on reaction kinetics from pressurized operation was confirmed also in this work. The reactivity of ilmenite ore over chemical looping combustion cycles with CO as fuel was investigated by Lu et al. in Ref. [45]. Increasing temperature and CO partial pressure resulted in an increase in reduction rate while increasing total pressure had the reverse effect. Similar results for methane fueled chemical looping combustion of ilmenite ore are reported by Tan et al. in Ref. [46]. On the oxidation side, Rana et al. analyzed the high pressure oxidation kinetics (with O_2) of ilmenite ore and confirmed the negative effect of total pressure, while constant O_2 volume fraction had a positive impact on kinetics up to a certain threshold. However, cracks formation was detected at high O_2 partial pressures. Finally, chemical looping combustion of methane and synthesis gas was investigated on Ni and Cu oxygen carriers at high pressure conditions (1–10 bar) by Nordness et al. [47]. Carbon deposition was observed to be promoted by pressure and the total pressure hindered the reduction rate. In contrast with the presented works, San Pio et al. [48] carried out high pressure chemical looping cycles of CuO/Al_2O_3 and demonstrated that total pressure does not impact conversion kinetics nor the morphological and chemical structure of the oxygen carrier. The previous results were thus justified by suggesting the presence of mass transfer limitations in the setups.

In this work, a set of tests was carried out over a chemical looping process at ambient pressure to analyze NiFe oxygen carriers properties regarding oxygen transport ability and how parameters such as nickel content or temperature can affect

them. This is an interesting aspect of the applications that these materials can have in different processes such as reforming and subsequent H_2 production. Additionally, the materials were extensively tested in high pressure chemical looping cycles to provide useful data, currently missing in the literature, on the effect of high pressure operation on reactivity and possibly support future scale-up of the technology to the industrial level. The effect of different operating conditions, such as temperature, reducing gas composition, total pressure, and oxygen carrier material loading was presented and discussed. In both low and high-pressure tests, only the redox behavior of the oxygen carriers has been considered. Finally, long-term stability tests were also carried out to assess the activity change over many cycles. The materials were characterized by several techniques (Inductively Coupled Plasma Spectrometry, X-Ray Diffraction, Temperature Programmed Reduction, Scanning Electron Microscopy, Energy Dispersive X-Ray Analysis) and comparison was made between the fresh and spent material samples.

2. Material and method

2.1. Material synthesis and characterization

Materials with approximately 10%wt. Fe and with two different Ni loadings of 5%wt. and 12%wt. have been synthesized through a co-precipitation/impregnation route. The co-precipitation protocol started by preparing a solution combining 0.3 M aluminium nitrate and 1.5 M iron nitrate stocks to the desired proportion. Under vigorous stirring a 2 M sodium carbonate solution was added dropwise in a 30% volume excess over stoichiometric value to ensure proper precipitation. The pH was adjusted to 9 followed by a 2-h ageing period at room temperature. After the incubation period, the solution was filtered and washed to remove sodium traces. The material was then dried overnight and grounded (100–200 μm). The next step was calcination in a furnace to obtain oxides (at 1000 °C for 4 h with a 10 °C/min heating ramp). For the impregnation method, the co-precipitated materials were used as a support and loaded with nickel. 5 g of support was mixed with a nickel nitrate solution and stirred at room temperature until it turned into slurry, then dried and finally calcined at 875 °C for two hours with a 10 °C/min ramp. Before and after testing, the materials were characterized through diverse techniques to determine the quality of the synthesis and their functionality. Inductively Coupled Plasma (ICP-OES, with an ICP-OES Xpectroblue-EOP FMT 26 spectrophotometer) served to corroborate the amount of Fe and Ni present in them. Characterization results are compiled in Table 1, which contains the amount of Ni, Fe and Al in the materials. X-Ray diffraction (XRD) analysis was performed on both the oxidized and reduced material states to assess the material phases evolution over the chemical looping cycles. The oxidized materials were 'as produced', while the other ones were reduced in a H_2/N_2 atmosphere in the two setups. Material reducibility was assessed through Temperature Programmed Reduction tests (TPR, AutoChem II 2920 from Micromeritics) that consisted in heating up the sample with a relatively low heating ramp (10 °C/min) in a 10% vol. H_2 in an Ar stream from room temperature up to 950 °C while measuring H_2 consumption. Finally, the morphology evolution and the fresh material homogeneity were investigated through Scanning Electron Microscopy (SEM) and Energy Dispersive X-Ray (EDX) scans.

Table 1 – Composition of the two synthesized NiFe aluminates from ICP-OES.

Batch	Ni	Fe	Al
1	4.3%	9.9%	41%
2	12%	8.5%	36%

2.2. Calculation method

The reaction performance of the materials was assessed by calculating the oxygen transport capacity (OTC) and the reduction conversion from the observed mass change in the two thermogravimetric analyzer (TGA) setups. The oxygen transport capacity represents the fraction of oxygen in the fresh material that is extracted by the gases and it was calculated according to Eq. (1).

$$OTC = \frac{m_{O_2}}{m_{ox}} = \frac{m_{ox} - m(t)}{m_{ox}} \quad (1)$$

Where:

- m(t) is the net sample mass at time t;
- m_{ox} is the net sample mass at the end of the oxidation step;

All data are corrected by the blank test before performing any calculations.

The instantaneous oxygen carrier reduction conversion X(t) is useful to assess the reduction kinetics of the materials under different operating conditions and it was computed according to Eq. (2)

$$X(t) = \frac{m_{ox} - m(t)}{m_{ox} - m_{red}} \quad (2)$$

Where m_{red} is the completely reduced sample mass (calculated with stoichiometry from m_{ox}).

2.3. Ambient pressure TGA setup

For ambient pressure tests, a thermogravimetric analyzer (TGA-CI Electronics Ltd.) was used to determine the materials chemical and mechanical stability under oxidizing and reducing conditions. This equipment consists of two concentrically arranged quartz tubes located inside a furnace. Each sample was introduced in a platinum basket placed at the bottom of this device. The apparatus is equipped with gas mass flow controllers that allow feeding H_2, CO, CH_4, O_2 and N_2. A thermocouple is located at the bottom of the setup for optimal temperature regulation. More details on the setup geometry can be found in Ref. [49]. In this TGA, 25 mg of material are manually loaded in a platinum crucible. The chemical looping cycles consisted of a 7 min reduction stage in a 20% H_2/N_2 atmosphere and a 5 min oxidation stage in 20% O_2/N_2. Intermediate purge of 1 min with N_2 was carried out to

prevent reactive gases mixing, while continuous flushing with N_2 was provided in the balance head to prevent the gases from entering it.

2.4. *High-pressure TGA setup*

For high-pressure chemical looping tests, a high-pressure thermogravimetric analyzer (HP-TGA) was used. A schematic layout of the setup is provided in Fig. 1. It consists of mass flow controllers for the reacting gases, a water vaporizer, a backpressure controller, pressure and temperature sensors and a microbalance (model MK2-5 M from CI-Precision). The microbalance has a sensitivity of 0.1 μg, a maximum capacity of 5 g and +/− 500 mg operating range. The setup can operate at pressures and temperatures up to 30 bar and 1100 °C, respectively. Air, CO, CO_2, CH_4, H_2O, H_2, N_2 are the available gases for testing. The balance is connected to a porous basket made of alumina (40 μm pores) through an Ir wire. A robotic lift is used to bring the basket outside the reactor to load it with the sample. The temperature in the reactor is controlled using a thermocouple positioned close to the sample to ensure stable conditions, while the temperature of the balance head is kept constant and is continuously purged with N_2 as a protection measure.

Prior to the test, the oxygen carrier is loaded into the basket. The sample weight used for the experiments is about 30 mg. After loading the sample, the basket is inserted in the reactor by the robotic lift and then the desired temperature and pressure conditions are imposed. Before testing the material at the desired conditions, preliminary activation cycles with reduction and oxidation steps are carried out. The reduction step (20 min) involves H_2/N_2, while the oxidation step (20 min) is carried out with 100% air. Between each reaction segment 100% N_2 is purged for 2 min to avoid reactant mixing. To ensure the reliability of the results, each chemical looping cycle is repeated at least 3 times and the data from the last cycle are used for post processing. The authors decided to focus more on the redox properties of the material and on the different behaviour at ambient and high-pressure conditions rather than on the reducing gas composition. Also, the presence of CO in the reducing gas mixture caused in many cases carbon deposition, especially at high-pressure. The tests were mainly performed at a total pressure of 20 bar, which is typical for chemical looping applications [50]. Blank tests were performed under the same operating conditions to remove the effect of buoyancy on the basket due to the changes in the feed gases and reactor temperature [51].

3. Results and discussion

3.1. *Ambient pressure chemical looping tests*

The two NiFe aluminates were subjected to reduction/oxidation cycles under isothermal conditions to determine their oxygen transport capacity and reduction conversion along multiple reaction cycles in a range of temperatures between 700 and 900 °C with 0.5 NL/min total flow rate. This set of experiments carried out at ambient pressure focused on the effect of temperature along the redox cycles. Up to 20 cycles were performed for each temperature to assess how oxygen transport capacity evolved in each material. As shown in Fig. 2 (a) and (b), the OTC behavior along the cycles is dependent on the temperature. At 720 °C the OTC decreases with the cycles and

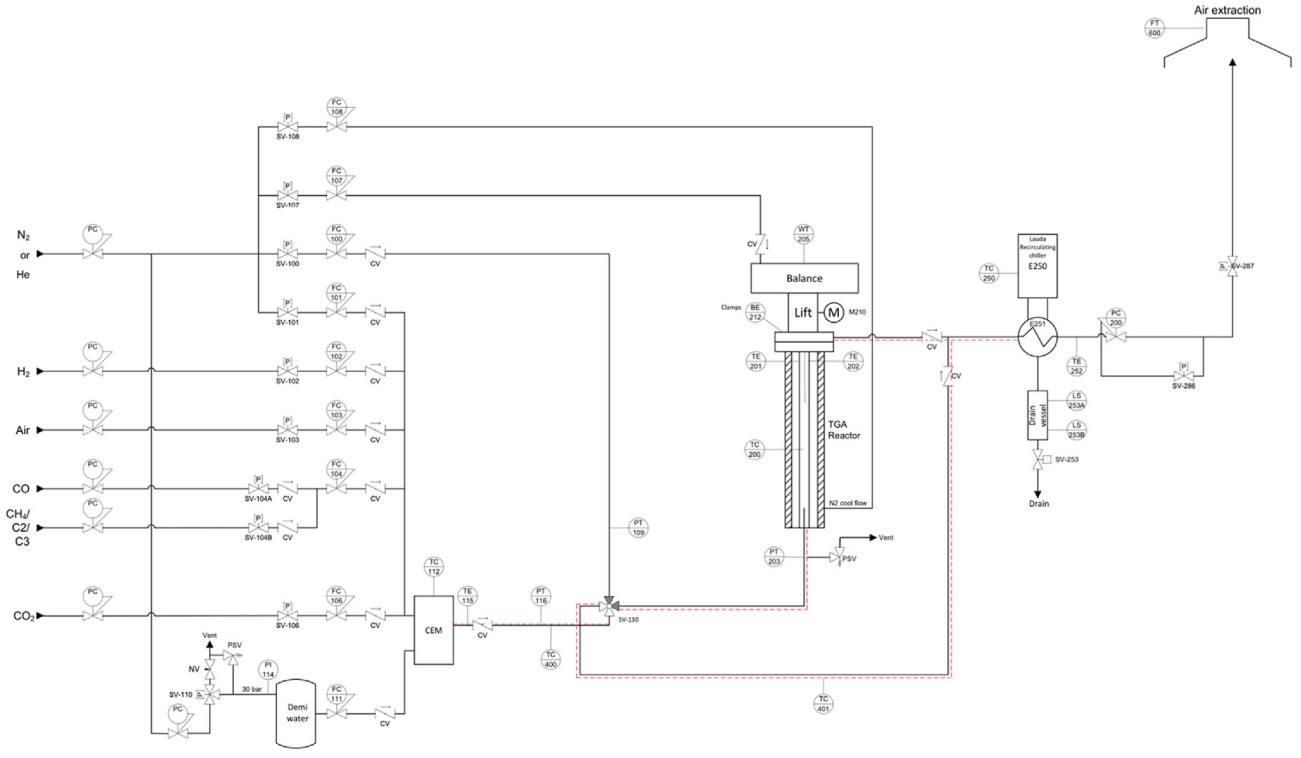

Fig. 1 – P&ID of the experimental apparatus for HP-TGA.

after the 5th cycle reaches stability. Similarly, at 820 °C the OTC increases and then from the 10th cycle it presents a plateau. On the contrary, for higher temperature values the OTC shows an increasing trend with the cycles. As expected, batch 2 (which has a higher amount of Ni) presented higher OTC values compared to batch 1. For example, at 900 °C the OTC of batch 2 NiFe aluminate is about twice the value of batch 1.

In Fig. 2 (c) and (d), the evolution of reduction conversion with time is represented and compared at different temperature levels. Only the results for cycle 20 are displayed since the materials present a more stable OTC at that point. For batch 1 material, reduction conversion was around 19% at 720 °C increasing up to 67% at the highest temperature tested. In batch 2, the temperature is still crucial in reduction phase but reduction conversion values ranged from 35% at 700 °C to full (100%) conversion at 900 °C. In this last case, full conversion is achieved in less than 200 s. The effect of temperature is thus more significant on batch 2 material compared to batch 1. The stronger interaction of Ni and Fe with the Al_2O_3 support for the material with lower Ni content could be responsible of this behavior. The absence of NiO species shown in XRD and TPR (see the material characterization section) corroborate the TGA results.

3.2. *High-pressure chemical looping tests*

Before investigating the high-pressure redox behavior of the NiFe aluminates, the HP-TGA setup was validated with a 12.5 wt% CuO/Al_2O_3 powder (1.1 mm diameter provided by Sigma Aldrich) at 800 °C and the results were compared with literature data [48]. Two tests were carried out at 6 bar, 3 NL/min and 4 NL/min total flow rate and 50% H_2/N_2 mixture. The plots of Figs. S1 and S2 of the Supplementary Material show a good agreement and ensure the safe and good operation of the HP-TGA. In the 4 NL/min comparison a larger deviation from literature data is observed, though it is expected that reduction conversion would constantly increase with time throughout the test.

In the following high-pressure experimental campaign, batch 1 NiFe aluminate was tested under different operating conditions i.e., flow rate, temperature, gas composition and pressure, to assess the influence of these parameters on reduction conversion at high pressure. A comparison with batch 2 material conversion under specific conditions was also carried out. Subsequently, the long-term stability of batch 2 material was investigated throughout 80 high-pressure cycles and compared with the results for 100 cycles at ambient pressure conditions.

3.2.1. *High-pressure reactivity of the NiFe aluminates*

The measurements were carried out at 800 °C, 20 bar and four flow rates of 2 NL/min, 4 NL/min, 6 NL/min and 8 NL/min (50% H_2/N_2) on batch 1 NiFe aluminate, and the results for reduction conversion are plotted in Fig. 3. At 2 NL/min, the system presents mass transfer limitations causing initially a slower reaction rate and a lower total conversion at the end of the test.

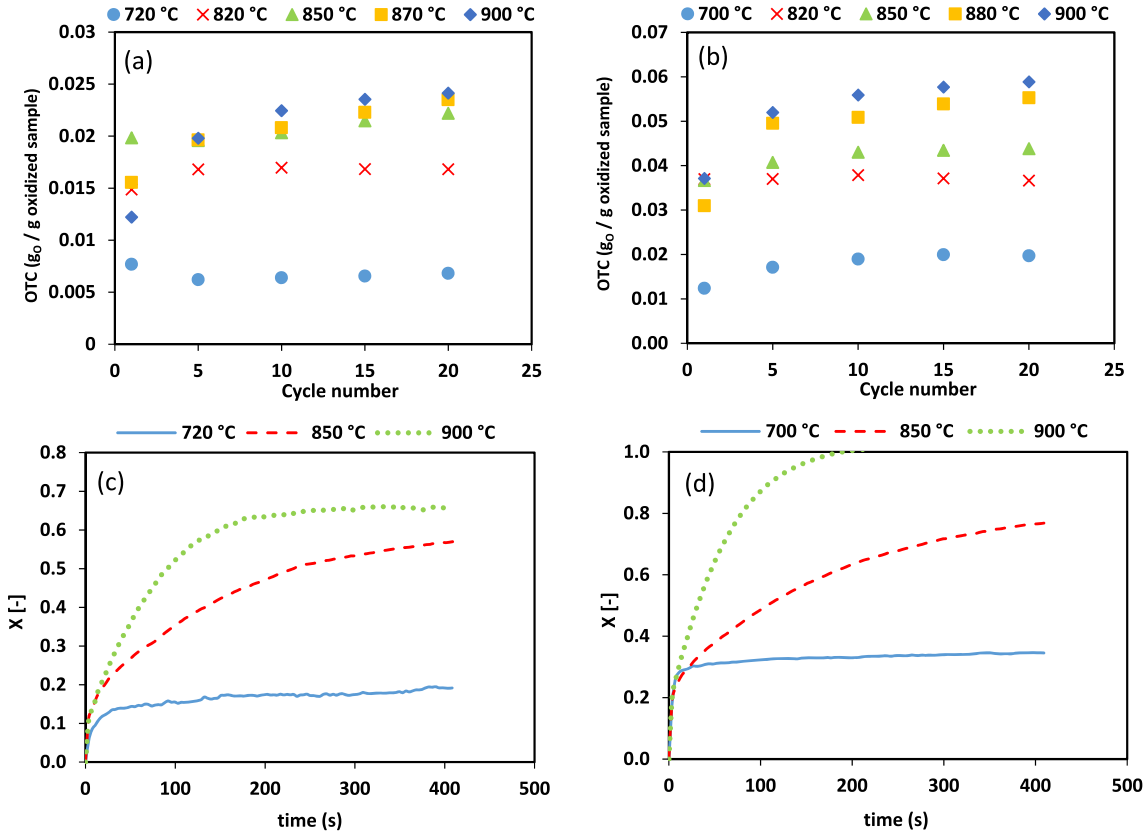

Fig. 2 – Oxygen transport capacity along reduction-oxidation cycles and reduction conversion at cycle 20 at different temperatures from batch 1 (a and c) and batch 2 (b and d).

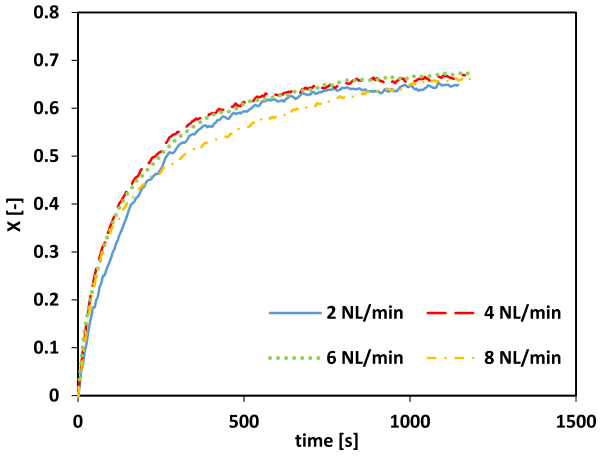

Fig. 3 – Reduction conversion of batch 1 NiFe aluminate at 20 bar, 800 °C and different flow rates.

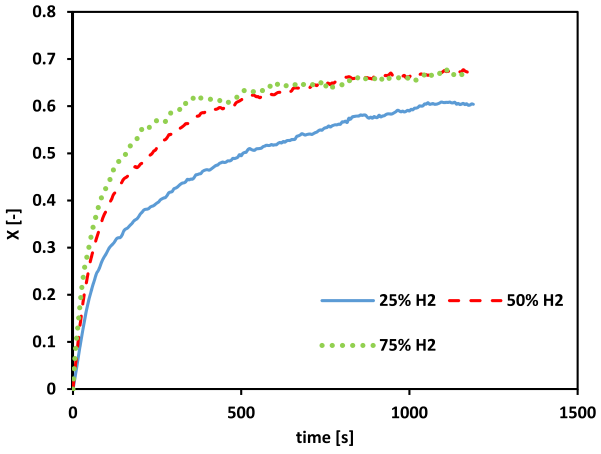

Fig. 5 – Reduction conversion of batch 1 NiFe aluminate at 20 bar, 800 °C, 6 NL/min and different H_2/N_2 mixtures.

On the contrary, almost the same initial reaction rate is observed for flow rates larger or equal than 4 NL/min with a similar final conversion of about 67%. This indicates that from 4 NL/min the system is not mass transfer limited.

The influence of temperature on batch 1 material reduction was then assessed. Tests were carried out at 6 NL/min, 20 bar and four temperature levels. A 50% H_2/N_2 reducing gas mixture was used in all tests. As it was described for material testing at atmospheric pressure, reducing temperature impacts in a significant way on final conversion as given in Fig. 4. The final conversion at 700 °C amounts to about 38% and is significantly lower compared to the other temperatures. At 750 °C, the reaction rate increases and a final conversion of about 61% is achieved. Above 800 °C, a similar final reduction conversion is reached, and the initial reduction rate increases with temperature.

The effect of the reducing gas composition on batch 1 reduction was assessed by using different mixtures of N_2 and H_2. Tests were carried out at 20 bar, 800 °C, 6 NL/min and three H_2/N_2 mixtures containing 25%, 50% and 75% H_2. The results are plotted in Fig. 5. Since a constant total pressure of 20 bar was imposed, different H_2 percentages in the mixtures correspond to different H_2 partial pressures in the reactor. For this reason, when the H_2 content was 25% H_2, a slower reaction rate and a lower final conversion were achieved. A still increasing trend is observed at the end of the 25% H_2 test, meaning that the conversion was proceeding still. For the other compositions a similar final conversion was achieved but with a faster kinetics for higher H_2 contents, as expected.

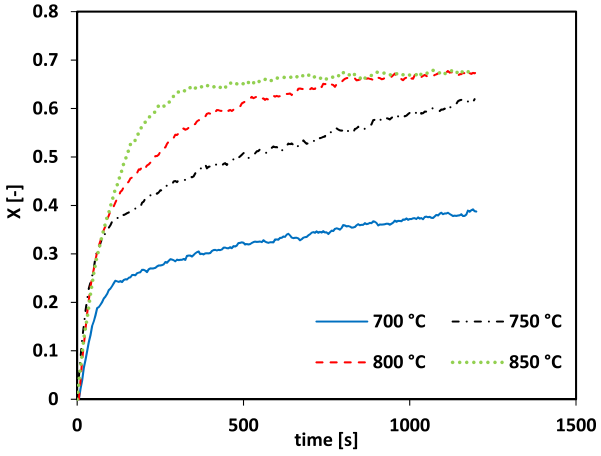

Fig. 4 – Reduction conversion of batch 1 NiFe aluminate at 20 bar, 800 °C, 6 NL/min and different temperature levels.

The effect of total pressure was investigated by fixing the hydrogen partial pressure $p_{H2} = 10$ bar while changing the total pressure in the system. The reduction conversion trends at 10, 15 and 20 bar are plotted in Fig. 6. The presence of a certain noise level in the 10 bar trend is associated with the utilization of pure H_2 ($p_{H2} = 10$ bar), for which the back pressure controller has difficulties in maintaining stable pressures. By comparing the plots, lower total pressure levels enhance the reaction rate and then approximately the same final conversion was achieved for the three cases. This confirms the negative effect of pressure on reduction kinetics, as detected in other literature works [43–47]. Several explanations have been provided to justify this phenomenon, mainly focusing on the slower products diffusion when leaving the particle surface, which then makes it more difficult for the fresh reactants to reach the active sites.

To further corroborate this observation, another test was carried out at 6 NL/min, 800 °C and 50% H_2/N_2 mixture with different total pressures in the system i.e., different H_2 partial pressures in the reactor. The results are plotted in Fig. 7. In these conditions, the negative effect of the total pressure is counterbalanced by the positive effect of higher partial pressures in the system. Hence, at 25 bar a slower initial reaction kinetics is observed compared to the 15 bar case, while comparable final conversions are achieved at the end of the test. The 20 bar plot shows a slightly better reduction rate along the whole 20 min reduction.

A comparison with batch 2 NiFe aluminate was carried out to see the effect of higher Ni loadings on reduction conversion. As can be seen in Fig. 8 the material shows a similar reduction behavior to that of batch 1 NiFe aluminate, which is

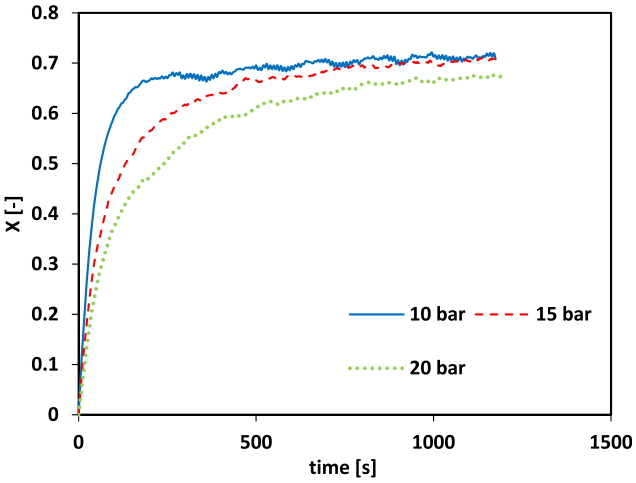

Fig. 6 – Reduction conversion of batch 1 NiFe aluminate at 800 °C, 6 NL/min, p_{H2} = 10 bar and different total pressures.

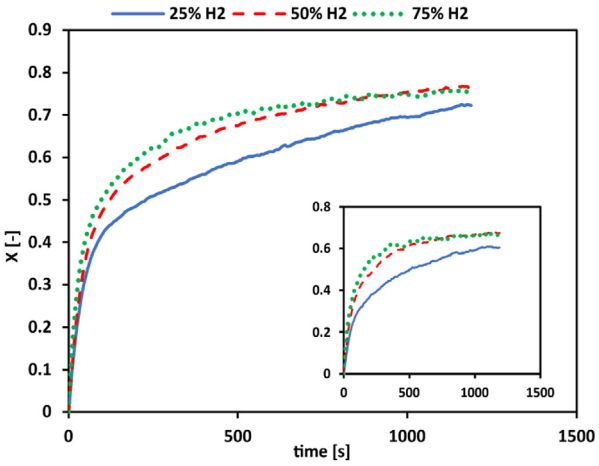

Fig. 8 – Reduction conversion of batch 2 NiFe aluminate at 20 bar, 800 °C, 6 NL/min and different H_2/N_2 mixtures.

represented in the detail of Fig. 8 for comparison. Increasing H_2 contents in the mixture, the reaction kinetics is enhanced. About the same final conversion (75%) is achieved for the 50% and 75% H_2 mixtures, while for the 25% H_2 case the conversion is generally lower throughout the test, but still increasing at the end of the test (about 72%). As already observed in Fig. 2 at ambient pressure, also at 20 bar a larger Ni content improves the reduction kinetics.

3.2.2. *Long-term stability*

The long-terms stability of the materials is an important aspect to be considered for scale up of the chemical looping technology. Two sets of runs were performed for ambient and high-pressure conditions on batch 2 NiFe aluminate, which has proved better reaction performance.

At ambient pressure, the long-term stability was assessed by performing approximately 100 redox cycles at 900 °C following the same conditions previously described. Fig. 9 shows that reduction conversion was not complete in the first cycles, but it improved later until it reaches (after cycle n. 40) a stable full conversion. These results were consistent with the increase of OTC shown in Fig. 2 when the material was submitted to consecutive cycles. However, the effect on the reduction conversion curve in early moments of the reaction (see 20 s detail in Fig. 9) was the opposite, i.e. the reaction was slightly slower in later cycles compared with the first ones but the decrease was quite low between cycle 40 and 70 and stable after that point.

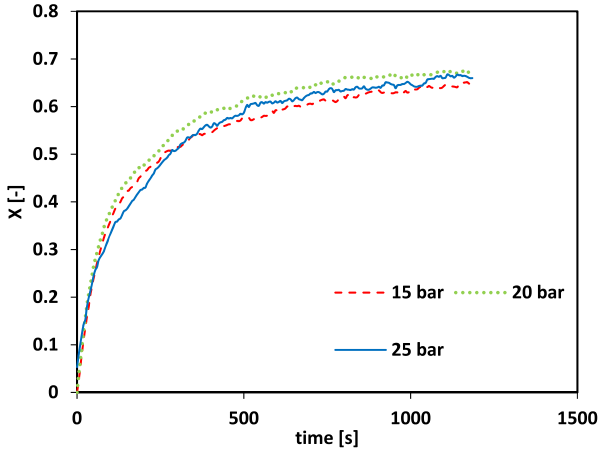

Fig. 7 – Reduction conversion of batch 1 NiFe aluminate at three total pressures, 800 °C, 6 NL/min and 50% H_2/N_2.

The reduction conversion trend throughout 80 chemical looping cycles at 20 bar was plotted in Fig. 10. The detail in Fig. 10 shows that after the first redox cycle, the initial slope of the reduction curve decreases over the cycles. On the contrary, the reduction conversion increases steadily until the 60th cycle. This "activation" phenomenon was also observed in other works on chemical looping with perovskites [52,53] and could be associated with an increase in specific surface area/porosity of the oxygen carrier as well as a change in the active phase after each oxidation step i.e. the aluminates are not regenerated.

3.2.3. *Material characterization*

Fresh materials reducibility was assessed through TPR tests. As shown in Fig. 11, the materials present an important consumption peak between 730 °C and 830 °C. There is also a H_2 consumption peak at lower temperatures (around 400 °C) that is more evident for the material with higher Ni loadings. This consumption peak is typical for the reduction of NiO with low interaction with the support [54]. In general, it has been observed that materials with lower Ni load present a higher interaction with the support or higher presence of $NiAl_2O_4$ that reduces at higher temperatures. This observation was confirmed by TPR and XRD tests.

The fresh materials from batch 1 and 2 have been characterised through SEM-EDX (Hitachi S-3400-N) at crosscut to assess the dispersion of Fe and Ni within the particles. The results, including the EDX line-scan data, are shown in Fig. 12. For batch 1 material, the Fe content is about twice the Ni content, as corroborated by ICP results previously discussed and shown in Table 1. On the contrary, for batch 2 the Fe and

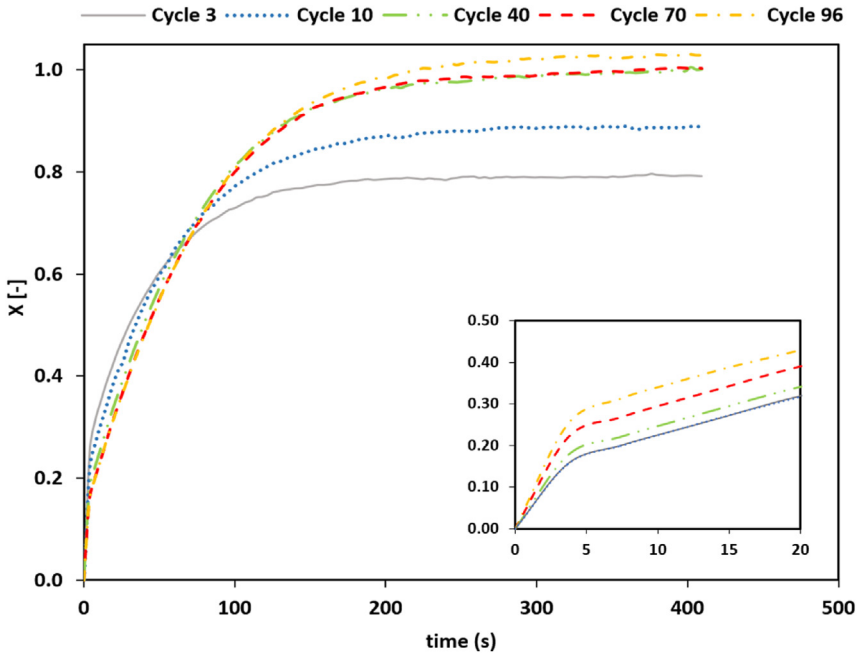

Fig. 9 – Reduction conversion of batch 2 NiFe aluminate at 900 °C and ambient pressure along multiple redox cycles.

Ni loadings are similar. All elements show homogeneous distribution within the particle, indicating that the support impregnation was successfully achieved.

SEM pictures (Thermo Scientific Phenom ProX) of the fresh batch 2 material and reduced after the 80 high-pressure cycles are compared in Fig. 13. In general, the microstructure of the spent material does not display particular signs of stress in terms of increased cracks or voids formation compared to the fresh material. The presence of voids and cracks has been detected also in the fresh material and is probably associated with material synthesis and subsequent handling. Moreover, the particle size after reduction is almost preserved compared to the oxidized state.

The XRD (Bruker D-8 Advance) patterns of the fresh and the reduced materials at ambient pressure conditions are displayed in Fig. 14.

In both oxidized materials, the presence of Fe and Ni in aluminate form was appreciated, but in batch 2 (with a higher

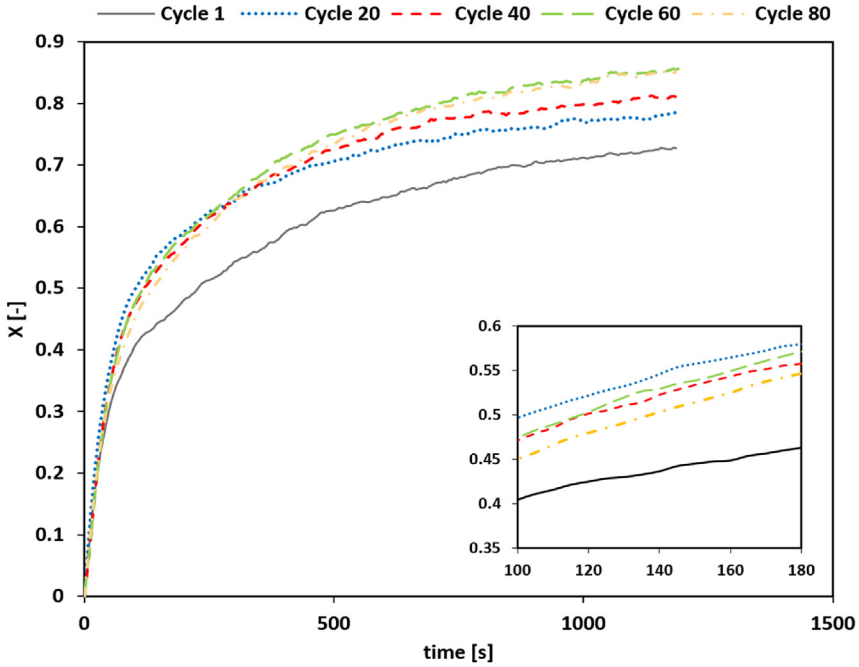

Fig. 10 – Reduction conversion of batch 2 NiFe aluminate at 20 bar along multiple redox cycles.

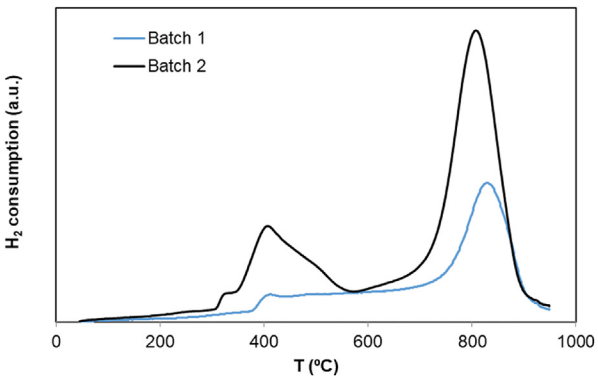

Fig. 11 – TPR data showing H_2 consumption up to 950 °C for materials from batch 1 and 2.

Ni content) NiO was also present as a Ni species. As the oxygen carriers have been submitted to a reduction atmosphere, peaks corresponding to an iron-nickel phase appeared. XRD patterns corresponding to the materials reduced at 820 °C and 900–920 °C showed the dependence of the reduction reaction with temperature. Samples reduced at the lowest temperature still have $FeAl_2O_4$ and $NiAl_2O_4$ peaks and Fe–Ni peaks of low intensity, while in samples reduced at high temperature the peaks corresponding to aluminates disappear and more intense Fe–Ni peaks are present. This confirms that under high temperature conditions the material was completely reduced, while only partial reduction took place at lower temperatures.

The XRD patterns (Rigaku MiniFlex) of the fresh and reduced material after long term tests (30 and 80 cycles) and at different pressure conditions (15 and 20 bar) are displayed in Fig. 15. In both cases, complete reduction conversion was not achieved. This is confirmed by the presence of aluminate phases peaks in all the reduced material patterns. As observed in by San Pio et al. in Ref. [55], the incomplete conversion could be attributed to the slower reaction kinetics of the aluminates compared to the Ni and Fe reduction or to the formation of other spinel structures. These patterns present a similar structure with three Fe–Ni peaks (around 44°, 52° and 76°). From the fresh material pattern, the oxidized phase peaks at 31° and 59° reduce in intensity, while the shoulder at 37° and the peaks at 56°, 66° disappear. No significant differences can be observed between the cycles n.30 and n. 80 of the reduced material patterns, as well as between 15 and 20 bar patterns. Therefore, the reaction pathway does not change either with pressure or along multiple cycles.

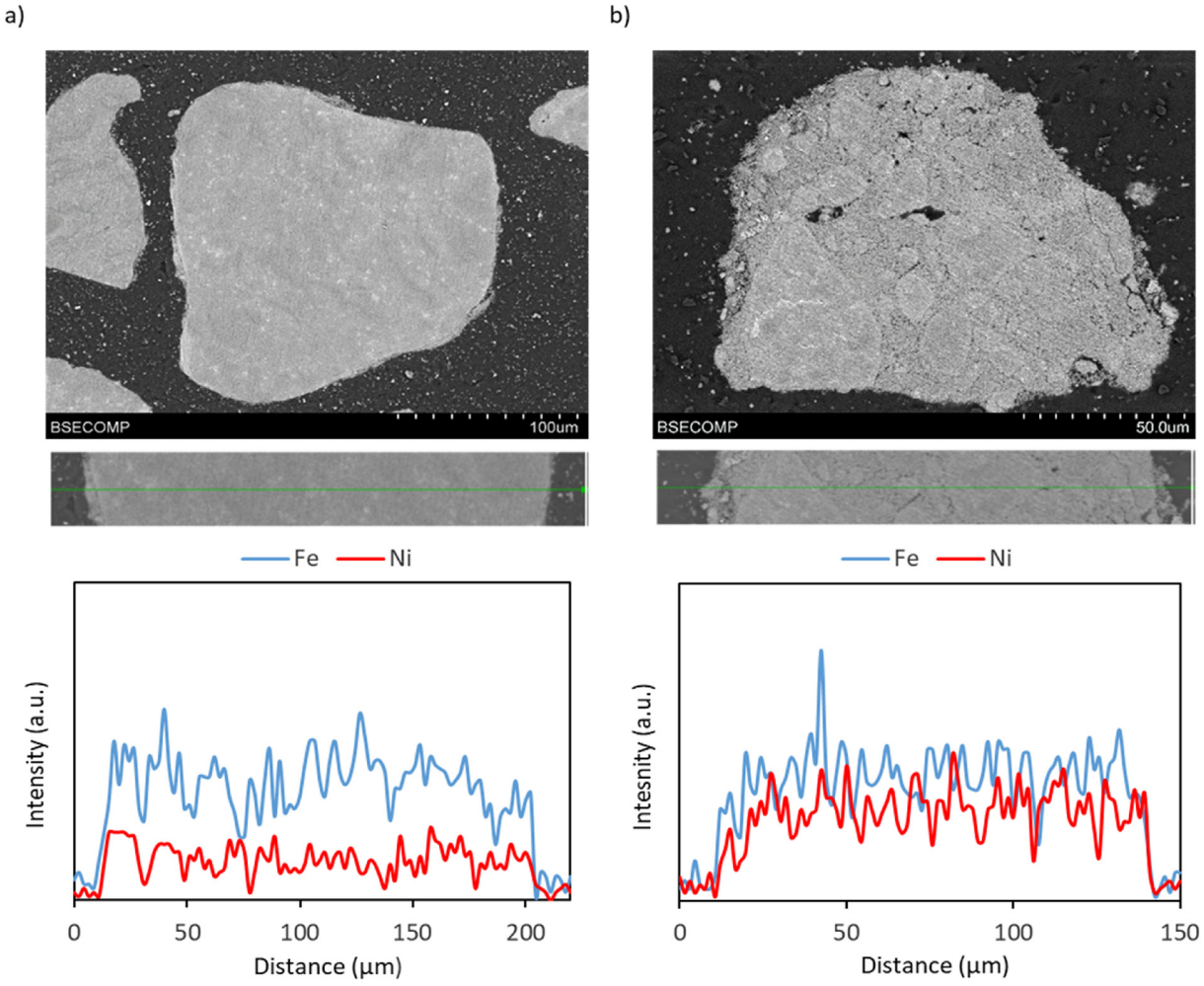

Fig. 12 – SEM images and EDX analysis with line-scan information for batch 1 (a) and batch 2 (b).

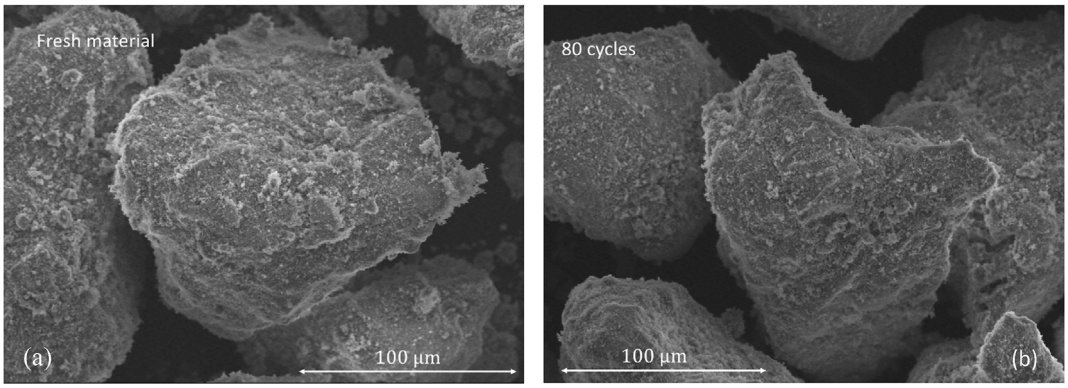

Fig. 13 – SEM pictures of fresh batch 2 NiFe aluminate (a) and reduced batch 2 after 80 high-pressure cycles (b).

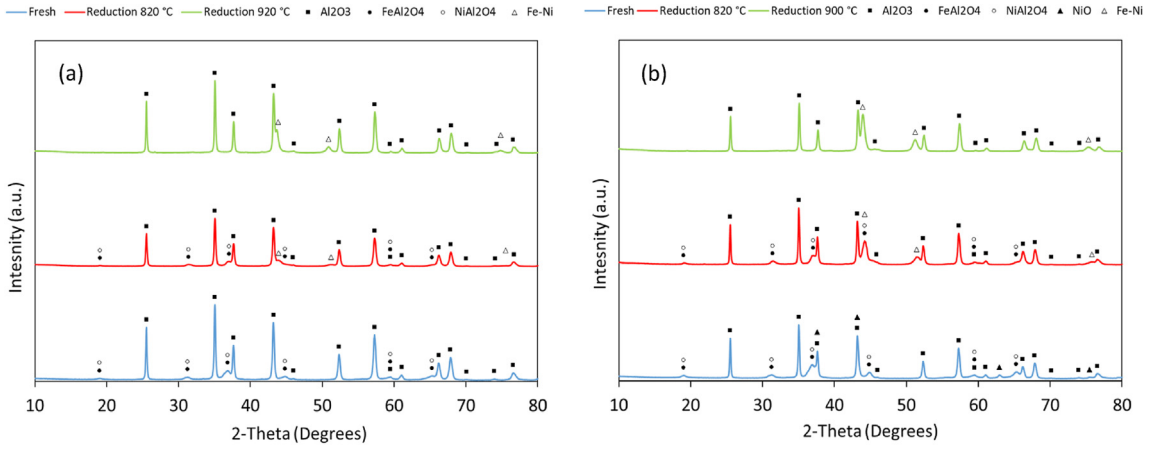

Fig. 14 – XRD patterns of batch 1 (a) and batch 2 (b) both fresh (oxidized) and reduced in H_2/N_2 at 820 °C and 900 °C or 920 °C.

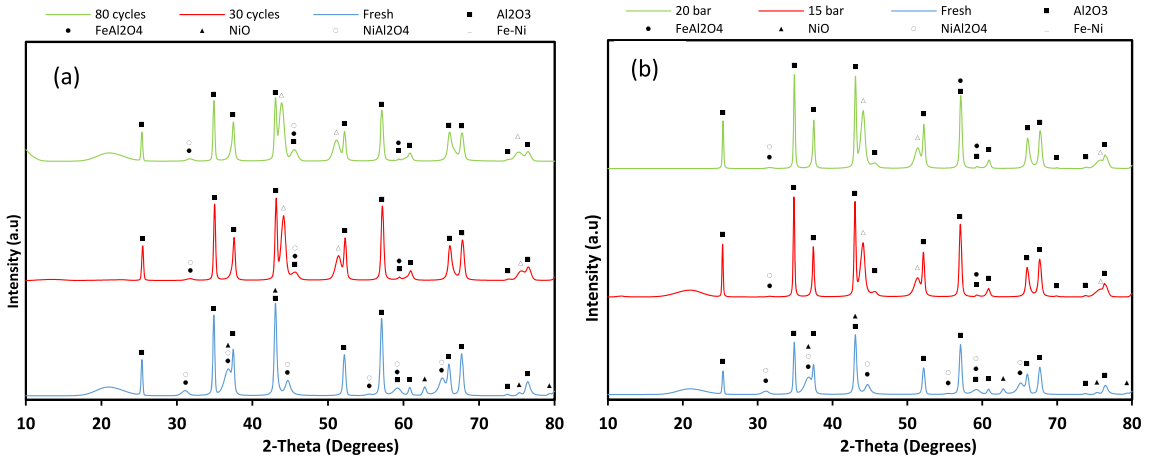

Fig. 15 – XRD patterns of batch 2 material fresh, reduced after 30 cycles (a) and 80 cycles (b) at 20 bar fresh, reduced at 15 bar and 20 bar with $p_{H2} = 10$ bar.

4. Conclusions

In this work, chemical looping cycles were carried out with two different setups to assess and compare the reduction behavior of two NiFe aluminates (batch 1 and 2) at ambient and high-pressure conditions. At ambient pressure conditions, the effect of different temperature levels on the oxygen transport capacity and on the reduction conversion of both materials was assessed. Each condition was tested for 20

reduction/oxidation cycles. It was shown that the oxygen transport capacity increases with the cycles for temperatures above 800 °C and that higher Ni loadings provide better reaction performances. Full reduction conversion was achieved at 900 °C after 200 s of testing for loadings of 12% wt Ni and 8.5% wt Fe. At high-pressure conditions, the time variation of reduction conversion of batch 1 material was assessed under different operating conditions. The occurrence of external mass transfer limitations at 20 bar was preliminarily studied and prevented. In all tests, a general behavior was observed where an initial fast kinetics is replaced by a plateau at high conversions. Increasing temperatures as well as higher H_2 contents demonstrated to improve the reaction kinetics and to reach a conversion plateau earlier, though the final conversion achieved was approximately the same from above 800 °C or above 50% H_2 content. Moreover, the total pressure showed a negative effect on reaction kinetics. Batch 2 material with higher Ni loading (12% wt) was tested under different H_2 compositions. Increased final conversion (depending on the specific condition) was observed when compared to the batch 1 material. Long-term testing at both ambient and high-pressure conditions was then carried out over 100 and 80 cycles, respectively. A reduction gain was observed throughout the cycles and full conversion was achieved for batch 2 material at 900 °C and ambient pressure after the 40th cycle. Similar behavior was observed at 20 bars in terms of reduction gain and initial kinetics. No significant changes in the microstructure of the material were observed and the comparison between diffraction patterns of the reduced material after 30 and 80 cycles didn't show differences in the detected phases. Therefore, it can be concluded that the support is able to ensure the continuous operation of the material over many cycles, while a higher Ni content in the spinel structure is indicated for better reduction performance and high cyclability in the process.

Declaration of competing interest

The authors declare that they have no known competing financial interests or personal relationships that could have appeared to influence the work reported in this paper.

Acknowledgment

This project has received funding from the European Union's Horizon 2020 Research and Innovation Program under grant agreement No 884197 (GLAMOUR).

Nomenclature

CLC	Chemical Looping Combustion
c-YSZ	Yttria-Stabilized Cubic Zirconia
EDX	Energy Dispersive X-Ray
HP-TGA	High-Pressure Thermogravimetric Analyzer
ICP	Inductively Coupled Plasma
m_{ox}	Net sample mass at the end of the oxidation step after the basket signal removal
m_{red}	Completely reduced sample mass
m(t)	Net sample mass at time t after the basket signal removal
OTC	Oxygen Transport Capacity
SEM	Scanning Electron Microscopy
TGA	Thermogravimetric Analyzer
TPR	Temperature Programmed Reduction
t-PSZ	Partially Stabilized Tetragonal Zirconia
XRD	X-Ray Diffraction

Appendix A. Supplementary data

Supplementary data to this article can be found online at https://doi.org/10.1016/j.ijhydene.2023.09.235.

REFERENCES

[1] Ramezani R, Di Felice L, Gallucci F. A review of chemical looping reforming technologies for hydrogen production: recent advances and future challenges. J Phys: Energy 2023. https://doi.org/10.1088/2515-7655/acc4e8.
[2] Boot-Handford ME, Abanades JC, Anthony EJ, Blunt MJ, Brandani S, Mac Dowell N, et al. Carbon capture and storage update. Energy Environ Sci 2014;7:130–89.
[3] Wolf J, Anheden M, Yan J. Comparison of nickel-and iron-based oxygen carriers in chemical looping combustion for CO2 capture in power generation. Fuel 2005;84:993–1006.
[4] Kvamsdal HM, Jordal K, Bolland O. A quantitative comparison of gas turbine cycles with CO2 capture. Energy 2007;32:10–24.
[5] Muhich CL, Ehrhart BD, Al-Shankiti I, Ward BJ, Musgrave CB, Weimer AW. A review and perspective of efficient hydrogen generation via solar thermal water splitting, vol. 5. Wiley Interdiscip Rev Energy Environ; 2015. p. 261–87. https://doi.org/10.1002/wene.174.
[6] Abanades S, Flamant G. Thermochemical hydrogen production from a two-step solar-driven water-splitting cycle based on cerium oxides. Sol Energy 2006;80:1611–23. https://doi.org/10.1016/j.solener.2005.12.005.
[7] Tian H, Chaudhari K, Simonyi T, Poston J, Liu T, Sanders T, et al. Chemical-looping combustion of coal-derived synthesis gas over copper oxide oxygen carriers. Energy Fuel 2008;22:3744–55.
[8] Mattisson T, Johansson M, Lyngfelt A. The use of NiO as an oxygen carrier in chemical-looping combustion. Fuel 2006;85:736–47.
[9] Yu Z, Yang Y, Yang S, Zhang Q, Zhao J, Fang Y, et al. Iron-based oxygen carriers in chemical looping conversions: a review. Carbon Res Conv 2019;2:23–34. https://doi.org/10.1016/j.crcon.2018.11.004.
[10] Hu J, Poelman H, Marin GB, Detavernier C, Kawi S, Galvita VV. FeO controls the sintering of iron-based oxygen carriers in chemical looping CO2 conversion. J CO2 Util 2020;40:101216.
[11] Tijani MM, Aqsha A, Mahinpey N. Synthesis and study of metal-based oxygen carriers (Cu, Co, Fe, Ni) and their interaction with supported metal oxides (Al2O3, CeO2, TiO2, ZrO2) in a chemical looping combustion system. Energy 2017;138:873–82. https://doi.org/10.1016/j.energy.2017.07.100.
[12] Cabello A, Abad A, Mendiara T, Izquierdo MT, de Diego LF. Outstanding performance of a Cu-based oxygen carrier

impregnated on alumina in chemical looping combustion. Chem Eng J 2022:140484.
[13] Abdalla A, Mohamedali M, Mahinpey N. Recent progress in the development of synthetic oxygen carriers for chemical looping combustion applications. Catal Today 2023;407:21–51.
[14] Adánez J, De Diego LF, García-Labiano F, Gayán P, Abad A, Palacios JM. Selection of oxygen carriers for chemical-looping combustion. Energy Fuel 2004;18:371–7. https://doi.org/10.1021/ef0301452.
[15] Gayán P, Luis F, García-Labiano F, Adánez J, Abad A, Dueso C. Effect of support on reactivity and selectivity of Ni-based oxygen carriers for chemical-looping combustion. Fuel 2008;87:2641–50.
[16] Kidambi PR, Cleeton JPE, Scott SA, Dennis JS, Bohn CD. Interaction of iron oxide with alumina in a composite oxygen carrier during the production of hydrogen by chemical looping. Energy Fuel 2012;26:603–17. https://doi.org/10.1021/ef200859d.
[17] Damizia M, Bracciale MP, Anania F, Tai L, De Filippis P, de Caprariis B. Efficient utilization of Al2O3 as structural promoter of Fe into 2 and 3 steps chemical looping hydrogen process: pure H2 production from ethanol. Int J Hydrogen Energy 2023. https://doi.org/10.1016/j.ijhydene.2023.04.067.
[18] De Vos Y, Jacobs M, Van Der Voort P, Van Driessche I, Snijkers F, Verberckmoes A. Sustainable iron-based oxygen carriers for chemical looping for hydrogen generation. Int J Hydrogen Energy 2019;44:1374–91. https://doi.org/10.1016/j.ijhydene.2018.11.099.
[19] De Vos Y, Jacobs M, Van Driessche I, Van Der Voort P, Snijkers F, Verberckmoes A. Processing and characterization of Fe-based oxygen carriers for chemical looping for hydrogen production. Int J Greenh Gas Control 2018;70:12–21. https://doi.org/10.1016/j.ijggc.2018.01.007.
[20] Jerndal E, Mattisson T, Thijs I, Snijkers F, Lyngfelt A. Investigation of NiO/NiAl2O4 oxygen carriers for chemical-looping combustion produced by spray-drying. Int J Greenh Gas Control 2010;4:23–35. https://doi.org/10.1016/j.ijggc.2009.09.007.
[21] Dueso C, Abad A, García-Labiano F, De Diego LF, Gayán P, Adánez J, et al. Reactivity of a NiO/Al2O3 oxygen carrier prepared by impregnation for chemical-looping combustion. Fuel 2010;89:3399–409. https://doi.org/10.1016/j.fuel.2010.03.043.
[22] Bhavsar S, Veser G. Bimetallic Fe-Ni oxygen carriers for chemical looping combustion. Ind Eng Chem Res 2013;52:15342–52. https://doi.org/10.1021/ie400612g.
[23] Kuo YL, Hsu WM, Chiu PC, Tseng YH, Ku Y. Assessment of redox behavior of nickel ferrite as oxygen carriers for chemical looping process. Ceram Int 2013;39:5459–65. https://doi.org/10.1016/j.ceramint.2012.12.055.
[24] Evdou A, Zaspalis V, Nalbandian L. Ferrites as redox catalysts for chemical looping processes. Fuel 2016;165:367–78. https://doi.org/10.1016/j.fuel.2015.10.049.
[25] Huang Z, Deng Z, He F, Chen D, Wei G, Zhao K, et al. Reactivity investigation on chemical looping gasification of biomass char using nickel ferrite oxygen carrier. Int J Hydrogen Energy 2017;42:14458–70. https://doi.org/10.1016/j.ijhydene.2017.04.246.
[26] Wei G, He F, Zhao Z, Huang Z, Zheng A, Zhao K, et al. Performance of Fe-Ni bimetallic oxygen carriers for chemical looping gasification of biomass in a 10 kWth interconnected circulating fluidized bed reactor. Int J Hydrogen Energy 2015;40:16021–32. https://doi.org/10.1016/j.ijhydene.2015.09.128.
[27] Chen J, Zhao K, Zhao Z, He F, Huang Z, Wei G. Identifying the roles of MFe 2 O 4 (M=Cu, Ba, Ni, and Co) in the chemical looping reforming of char, pyrolysis gas and tar resulting from biomass pyrolysis. Int J Hydrogen Energy 2019;44:4674–87. https://doi.org/10.1016/j.ijhydene.2018.12.216.
[28] Wang X, Chen Z, Hu M, Tian Y, Jin X, Ma S, et al. Chemical looping combustion of biomass using metal ferrites as oxygen carriers. Chem Eng J 2017;312:252–62. https://doi.org/10.1016/j.cej.2016.11.143.
[29] Argyris PA, De Leeuwe C, Abbas SZ, Amieiro A, Poultson S, Wails D, et al. Chemical looping reforming for syngas generation at real process conditions in packed bed reactors: an experimental demonstration. Chem Eng J 2022;435:134883.
[30] de Leeuwe C, Abbas SZ, Argyris PA, Zaidi A, Amiero A, Poultson S, et al. Thermochemical syngas generation via solid looping process: an experimental demonstration using Fe-based material. Chem Eng J 2023;453:139791.
[31] Bracciale MP, Damizia M, De Filippis P, de Caprariis B. Clean syngas and hydrogen Co-production by gasification and chemical looping hydrogen process using MgO-doped Fe2O3 as redox. Material. Catalysts 2022;12. https://doi.org/10.3390/catal12101273.
[32] Ortiz M, de Diego LF, Abad A, Garcia-Labiano F, Gayan P, Adanez J. Catalytic activity of Ni-based oxygen-carriers for steam methane reforming in chemical-looping processes. Energy Fuel 2012;26:791–800.
[33] Huang Z, He F, Chen D, Zhao K, Wei G, Zheng A, et al. Investigation on reactivity of iron nickel oxides in chemical looping dry reforming. Energy 2016;116:53–63.
[34] Antzara A, Heracleous E, Silvester L, Bukur DB, Lemonidou AA. Activity study of NiO-based oxygen carriers in chemical looping steam methane reforming. Catal Today 2016;272:32–41.
[35] Luo M, Yi Y, Wang S, Wang Z, Du M, Pan J, et al. Review of hydrogen production using chemical-looping technology. Renew Sustain Energy Rev 2018;81:3186–214. https://doi.org/10.1016/j.rser.2017.07.007.
[36] Deshpande N, Majumder A, Qin L, Fan LS. High-pressure redox behavior of iron-oxide-based oxygen carriers for syngas generation from methane. Energy Fuel 2015;29:1469–78. https://doi.org/10.1021/ef5025998.
[37] Palone O, Hoxha A, Gagliardi GG, Di Gruttola F, Stendardo S, Borello D. Synthesis of methanol from a chemical looping syngas for the decarbonization of the power sector. J Eng Gas Turbines Power 2023;145:21018.
[38] Pereira RJL, Argyris PA, Spallina V. A comparative study on clean ammonia production using chemical looping based technology. Appl Energy 2020;280:115874.
[39] Roshan Kumar T, Mattisson T, Rydén M. Techno-economic assessment of chemical looping gasification of biomass for Fischer–Tropsch crude production with net-negative CO2 emissions: part 2. Energy Fuel 2022;36:9706–18.
[40] Osman M, Khan MN, Zaabout A, Cloete S, Amini S. Review of pressurized chemical looping processes for power generation and chemical production with integrated CO2 capture. Fuel Process Technol 2021;214. https://doi.org/10.1016/j.fuproc.2020.106684.
[41] Zhang S, Xiao R, Zheng W. Comparative study between fluidized-bed and fixed-bed operation modes in pressurized chemical looping combustion of coal. Appl Energy 2014;130:181–9. https://doi.org/10.1016/j.apenergy.2014.05.049.
[42] Gallucci F, Hamers HP, Van Zanten M, van Sint Annaland M. Experimental demonstration of chemical-looping combustion of syngas in packed bed reactors with ilmenite. Chem Eng J 2015;274:156–68.
[43] Hamers HP, Gallucci F, Williams G, Cobden PD, van Sint Annaland M. Reactivity of oxygen carriers for chemical-

looping combustion in packed bed reactors under pressurized conditions. Energy Fuel 2015;29:2656–63.
[44] Garcia-Labiano F, Adánez J, de Diego LF, Gayán P, Abad A. Effect of pressure on the behavior of copper-, iron-, and nickel-based oxygen carriers for chemical-looping combustion. Energy Fuel 2006;20:26–33.
[45] Lu X, Rahman RA, Lu DY, Ridha FN, Duchesne MA, Tan Y, et al. Pressurized chemical looping combustion with CO: reduction reactivity and oxygen-transport capacity of ilmenite ore. Appl Energy 2016;184:132–9. https://doi.org/10.1016/j.apenergy.2016.09.107.
[46] Tan Y, Ridha FN, Duchesne MA, Lu DY, Hughes RW. Reduction kinetics of ilmenite ore as an oxygen carrier for pressurized chemical looping combustion of methane. Energy Fuel 2017;31:7598–605. https://doi.org/10.1021/acs.energyfuels.7b01038.
[47] Nordness O, Han L, Zhou Z, Bollas GM. High-pressure chemical-looping of methane and synthesis gas with Ni and Cu oxygen carriers. Energy Fuel 2016;30:504–14. https://doi.org/10.1021/acs.energyfuels.5b01986.
[48] San Pio MA, Gallucci F, Roghair I, van Sint Annaland M. Gas-solids kinetics of CuO/Al2O3 as an oxygen carrier for high-pressure chemical looping processes: the influence of the total pressure. Int J Hydrogen Energy 2017;42:12111–21.
[49] Díez-Martín L, Martínez I, Grasa G, Murillo R. Investigation of the reduction kinetics of high loaded CuO-based materials suitable for the Ca/Cu looping process. Fuel 2018;230:376–89. https://doi.org/10.1016/j.fuel.2018.05.054.
[50] Chiesa P, Lozza G, Malandrino A, Romano M, Piccolo V. Three-reactors chemical looping process for hydrogen production. Int J Hydrogen Energy 2008;33:2233–45.
[51] Coenen K, Gallucci F, Cobden P, van Dijk E, Hensen E, van Sint Annaland M. Chemisorption working capacity and kinetics of CO2 and H2O of hydrotalcite-based adsorbents for sorption-enhanced water-gas-shift applications. Chem Eng J 2016;293:9–23.
[52] Cabello A, Abad A, Gayán P, García-Labiano F, de Diego LF, Adánez J. Increasing energy efficiency in chemical looping combustion of methane by in-situ activation of perovskite-based oxygen carriers. Appl Energy 2021;287. https://doi.org/10.1016/j.apenergy.2021.116557.
[53] Abad A, Cabello A, Gayán P, García-Labiano F, de Diego LF, Mendiara T, et al. Kinetics of CaMn0.775Ti0.125Mg0.1O2.9-δ perovskite prepared at industrial scale and its implication on the performance of chemical looping combustion of methane. Chem Eng J 2020;394. https://doi.org/10.1016/j.cej.2020.124863.
[54] Salhi N, Boulahouache A, Petit C, Kiennemann A, Rabia C. Steam reforming of methane to syngas over NiAl2O4 spinel catalysts. Int J Hydrogen Energy 2011;36:11433–9. https://doi.org/10.1016/j.ijhydene.2010.11.071.
[55] San Pio MA, Gallucci F, Roghair I, van Sint Annaland M. On the mechanism controlling the redox kinetics of Cu-based oxygen carriers. Chem Eng Res Des 2017;124:193–201. https://doi.org/10.1016/j.cherd.2017.06.019.